Atmospheric Environment 83 (2014) 43–52

Contents lists available at ScienceDirect

Atmospheric Environment

journal homepage: www.elsevier.com/locate/atmosenv

Optical properties and radiative forcing of urban aerosols in Nanjing, China

B.L. Zhuang [a], T.J. Wang [a,*], S. Li [a], J. Liu [a,b], R. Talbot [c], H.T. Mao [d], X.Q. Yang [a], C.B. Fu [a], C.Q. Yin [a], J.L. Zhu [a], H.Z. Che [e], X.Y. Zhang [e]

[a] School of Atmospheric Sciences, Nanjing University, Hankou Rd. 22, Nanjing 210093, China
[b] University of Toronto, Toronto M5S 3G3, Canada
[c] Department of Earth & Atmospheric Sciences, University of Houston, Houston, TX 77204, USA
[d] Department of Chemistry, State University of New York, College of Environmental Science and Forestry, Syracuse, NY 13219, USA
[e] Chinese Academy of Meteorological Sciences, Beijing 100081, China

HIGHLIGHTS

- Aerosol characteristics, optical properties and DRF were analyzed in urban Nanjing.
- BC accounted for about 6.6 ± 2.9% of $PM_{2.5}$ in urban Nanjing from Jan to Apr 2011.
- Wavelength-dependent surface albedo of MODIS was used when accessing aerosol DRFs.
- Annual 550 nm AOD was 0.04 and 0.6 for absorbed and total aerosols in Nanjing (NJ).
- Clear sky DRF of NJ-absorbed and total aerosols was +4.5 and −6.9 W m^{-2} at the TOA.

ARTICLE INFO

Article history:
Received 2 March 2013
Received in revised form
4 September 2013
Accepted 23 October 2013

Keywords:
Aerosols
Optical depth
Single scattering albedo
Angstrom exponent
Radiative forcing
Nanjing

ABSTRACT

Continuous measurements of atmospheric aerosols were made in Nanjing, a megacity in China, from 18 January to 18 April, 2011 (Phase 1) and from 22 April 2011 to 21 April 2012 (Phase 2). Aerosol characteristics, optical properties, and direct radiative forcing (DRF) were studied through interpretations of these measurements. We found that during Phase 1, mean $PM_{2.5}$, black carbon (BC), and aerosol scattering coefficient (Bsp) in Nanjing were 76.1 ± 59.3 μg m^{-3}, 4.1 ± 2.2 μg m^{-3}, and 170.9 ± 105.8 M m^{-1}, respectively. High pollution episodes occurred during Spring and Lantern Festivals when hourly $PM_{2.5}$ concentrations reached 440 μg m^{-3}, possibly due to significant discharge of fireworks. Temporal variations of $PM_{2.5}$, BC, and Bsp were similar to each other. It is estimated that inorganic scattering aerosols account for about 49 ± 8.6% of total aerosols while BC only accounted for 6.6 ± 2.9%, and nitrate was larger than sulfate. In Phase 2, optical properties of aerosols show great seasonality. High relative humidity (RH) in summer (June, July, August) likely attributed to large optical depth (AOD) and small Angstrom exponent (AE) of aerosols. Due to dust storms, AE of total aerosols was the smallest in spring (March, April, May). Annual mean 550-nm AOD and 675/440-nm AE were 0.6 ± 0.3 and 1.25 ± 0.29 for total aerosols, 0.04 ± 0.02 and 1.44 ± 0.50 for absorbing aerosols, 0.48 ± 0.29 and 1.64 ± 0.29 for fine aerosols, respectively. Annual single scattering albedo of aerosols ranged from 0.90 to 0.92. Real time wavelength-dependent surface albedo from the Moderate Resolution Imaging Spectroradiometer (MODIS) was used to assess aerosol DRFs. Both total and absorbing aerosol DRFs had significant seasonal variations in Nanjing and they were the strongest in summer. Annual mean clear sky TOA DRF (including daytime and nighttime) of total and absorbing aerosols was about −6.9 and +4.5 W m^{-2}, respectively. Aerosol DRFs were found to be sensitive to surface albedo. Over brighter surfaces, solar radiation was more absorbed by absorbing aerosols and less scattered by scattering aerosols.

1. Introduction

Atmospheric aerosols can influence global and regional climate significantly and their loadings have substantially increased since preindustrial times (Qin et al., 2001). Kiehl and Briegleb (1993)

* Corresponding author. Tel./fax: +86 2583593797.
E-mail address: tjwang@nju.edu.cn (T.J. Wang).

1352-2310
http://dx.doi.org/10.1016/j.atmosenv.2013.10.052

suggested that the sulfate aerosol direct effect could greatly offset the warming effect of CO_2 in regions with high sulfate concentrations and Jacobson (2002) emphasized the warming effect of black carbon (BC) as it is only preceded by CO_2, implying the importance of atmospheric aerosols on the global energy budget.

Aerosol optical and radiative properties at global and regional scales have been studied since 1990s with model simulations (Penner et al., 2001; Liao and Seinfeld, 2005; Zhuang et al., 2013a) and satellite/surface-based retrievals (Bellouin et al., 2003; Zhang et al., 2005; Christopher et al., 2006; etc.). Furthermore, uncertainties of internally/externally mixing states in estimating aerosol direct radiative forcings (DRFs) have been assessed with numerical models in the last decade (Jacobson, 2001; Kim et al., 2008; Zhuang et al., 2013b). Forster et al. (2007) estimated that the global mean aerosol DRF at the top of atmosphere (TOA) is about -0.55 W m^{-2}, derived from the ground observations, while the DRF value is positive from model simulation, i.e., $+0.04$ to -0.63 W m^{-2}. Reddy et al. (2005) suggested that the global mean simulated DRF of anthropogenic and natural aerosols at the TOA was about -2.1 W m^{-2} in clear sky. At region scale over East Asia, simulated DRF at the TOA is from -6.77 to -3.43 W m^{-2} for total aerosols (Huang et al., 2007), $+0.81$ W m^{-2} for BC (Zhuang et al., 2013a), and -0.88 W m^{-2} for nitrate (Wang et al., 2010). Generally, aerosol DRFs derived from ground observations have relatively lower uncertainties in comparison with those from simulations. Ramanathan and Carmichael (2008) found poorer performances in model simulations of aerosols over Southern Asia compared with observations. Recently, more and more observations have been used to study regional aerosol optical and radiative properties (Yu et al., 2006). For examples, Markowicz et al. (2008) found that the daily mean surface DRF can exceed -20 W m^{-2} in Persian Gulf region. Khatri et al. (2009) reported that summer aerosols in Nagoya have a high absorbing ability, resulting in a positive DRF of $+2.5$ W m^{-2} at the TOA and a very negative forcing of -71.8 W m^{-2} at the surface. In Kuhlmann and Quaas (2010), shortwave radiation was found to be reduced by 20–30 W/m^2 due to aerosol perturbation over Qinghai-Tibet Plateau. Alam et al. (2011) derived a mean aerosol DRF about -22 ± 6 W m^{-2} at the TOA in Karachi from observations.

China is one of the main source regions for atmospheric aerosols in the world. Aerosols over China vary complicatedly in compositions and distributions. Aerosols emit strongly in central, southwestern, and eastern China, including Yangtze River Delta (YRD) and Pearl River Delta regions (Zhang et al., 2009), one of the fastest growth regions over China. Although the aerosol direct effects over China have been studied in numerical simulations (Wu and Fu, 2005; Han et al., 2009, 2012, 2011; Han, 2010; H. Zhang et al., 2012) and in observations (Xia et al., 2007; Wang et al., 2009; Li et al., 2010; Yan et al., 2010; Cai et al., 2011; Bai et al., 2011; Xiao et al., 2011; Zhou et al., 2011), none of them derived the optical properties and DRF of urban aerosols in YRD from observations.

The objective of this study is to better understand the characteristics, optical properties, and DRFs of urban aerosols in YRD, with interpretations of short-term (three months) measurements of BC, aerosol scattering coefficient (Bsp), and particulate matters with diameter of 2.5 μm or less ($PM_{2.5}$) and long-term (one year) measurements of aerosols optical depth (AOD) and Angstrom exponent (AE) at an urban site in Nanjing, YRD. A column radiative transfer model, Tropospheric Ultraviolet–Visible radiation model (TUV) (Madronich, 1993) was employed to calculate clear sky aerosol DRFs at the TOA and the surface. In previous studies, surface albedo for solar broadband or visible albedo was often used in estimating aerosol DRFs (Ma and Yu, 2012). In this study, wavelength-dependent surface albedo from the Moderate Resolution Imaging Spectroradiometer (MODIS) satellite instrument was used.

This paper is organized as follows. The method including the measurements and the radiation transfer model TUV is described in Section 2. The measured data are interpreted in Section 3, regarding the characteristics of aerosols in Nanjing in Section 3.1, optical properties of aerosols in Section 3.2, and aerosol direct radiative forcing Section 3.3. Conclusions are provided in Section 4.

2. Methods

2.1. Observation site, instrument and data introductions

Nanjing is the capital city of the Jiangsu province, a typical developing city of YRD. The sampling site is located in the downtown area of the city inside the Gulou campus of Nanjing University, at 32.05 °N, 118.78 °E, with the altitude of 99.3 m (79.3 m building tall plus 20 m asl), There are no higher buildings near or around the site. More details about the station are available in Zhu et al. (2012).

Short-term measurements of $PM_{2.5}$, BC and Bsp were made from 18 January 2011 to 18 April 2011 (defined as Phase 1). These three variables were measured with TEOM particulate mass monitor-Series 1400, Aethalometer (AE-31), and Integrating Polar Nephelometer with $PM_{2.5}$ size-cut inlet sensors (NGN-3A) (shown in Table 1). To obtain the compositions of total aerosols, Ambient Eight Stage Cascade Impactor Sampler was used.

Total aerosols AOD and AE were measured for a longer period from 22 April 2011 to 21 April 2012 (defined as Phase 2) using a Cimel sunphotometer CE-318N. Additionally, single scattering albedo (SSA) of total aerosols and AODs of absorbing, fine, and coarse aerosols could be inversed by DOBVIC algorithm which has been used in Aerosol Robotic Network (AERONET).

Relative humidity was measured with a conventional meteorological instrument at the site. Wind direction and speed were acquired from the national meteorological station which is about 1.5 km far away from the site.

Table 1
Introductions on the sampling instruments of aerosols.

Instruments	Factor (unit)	Method	Range	Resolution	Accuracy
I1	$PM_{2.5}$ mass (μg m^{-3})	A tapered element oscillating microbalance	>0.01 μg m^{-3}	0.01 μg m^{-3}	1 min
I2	BC mass (μg m^{-3})	Attenuation of transmitted light through membrane with BC	0–1 mg m^{-3}	0.001 μg m^{-3}	5 min
I3	Bsp (M m^{-1})	Irradiation to the particles of sampling gases using internal light source	0.1–3276.8 M m^{-1}	0.1 M m^{-1}	2 min

I1TEOM particulate mass monitor, Series 1400.
I2Aethalometer (AE-31).
I3Integrating Polar Nephelometer with $PM_{2.5}$ size-cut inlet sensors (NGN-3A).

2.2. Radiation transfer model

Using observed aerosol optical properties (including AOD, SSA, and AE) and the surface albedo, we can calculate aerosol DRF in Nanjing with the TUV model (Madronich, 1993). Aerosol DRF is highly dependent on aerosol column burden and compositions so that AOD and SSA are the dominant factors controlling aerosol DRFs. The surface albedo is another influential factor (Ma and Yu, 2012). Therefore, wavelength-dependent hourly aerosol AOD, SSA, AE, and the daily surface albedo observed during Phase 2 were used to substitute the original default values in TUV when estimating the shortwave radiative flux with the presence of aerosols in Nanjing. The solar component of the radiative transfer scheme in TUV follows the δ-Eddington approximation. The default aerosol attenuation coefficient profile used in the model is available in Palancar and Toselli (2004). Cloud covers were not considered here because all the aerosol optical properties were observed only under a clear sky condition. Aerosol radiative forcing here is defined as an instantaneous forcing: the difference between net shortwave radiative flux with aerosols and that without aerosols at the TOA or at the surface. Gas absorptions in the atmosphere were set to be constant (in default values).

3. Results and discussions

3.1. Characteristics of urban aerosols in Nanjing

Fig. 1 shows the time series of hourly mean concentrations of BC, $PM_{2.5}$, and 550-nm aerosol scattering coefficient (Bsp) during Phase 1, suggesting similar temporal variations in the atmospheric species (BC and $PM_{2.5}$) and the aerosol parameter (Bsp). Mean values of BC, $PM_{2.5}$, and 550-nm Bsp were 4.1 μg m^{-3}, 76.1 μg m^{-3}, and 170.9 M m^{-1}, respectively, with corresponding standard deviations of 2.2 μg m^{-3}, 59.3 μg m^{-3}, and 105.8 M m^{-1}. BC, $PM_{2.5}$, and Bsp followed a typical lognormal pattern (not shown). More than 60% of the samplings were within ranges from 1 to 5 μg m^{-3} for BC, 30 to 120 μg m^{-3} for $PM_{2.5}$ and 60 to 180 M m^{-1} for Bsp during Phase 1. High pollution episodes appeared in early and middle February in Chinese Spring and Lantern Festivals, possibly due to the significant local discharge of fireworks and relatively small wind speeds (see discussion on Fig. 2b). The maximum value reached 12 μg m^{-3} for BC, 400 μg m^{-3} for $PM_{2.5}$, and 500 M m^{-1} for Bsp during the period. BC accounted for about 6.6 ± 2.9% of total $PM_{2.5}$.

The mean diurnal variations of aerosol during Phase 1 show peaks at rush hours (8:00–9:00 am and pm LST), when the hourly-mean values reached 4.7 μg m^{-3}, 89.7 μg m^{-3} and 185.7 M m^{-1} for BC, $PM_{2.5}$, and Bsp, respectively (Fig. 2a). Although there are no large industrial pollution sources within a 30 km radius of the site, several main roads with heavy traffics surround the site (Zhu et al., 2012). The diurnal variations of vehicle volumes (not shown) on these roads also show two peaks in early morning and evening. Low level aerosol concentrations appeared in predawn in nighttime and at 13:00–14:00 pm in daytime because aerosol emissions were weak in the nighttime and boundary layers were well developed in the afternoon. However, this normal diurnal cycle could be altered in polluted episodes, such as in Lantern Festival when aerosol concentrations were relatively low in the daytime on 17 Feb 2011 but became dramatically high in the nighttime (Fig. 2b). BC, $PM_{2.5}$, and Bsp increased by about 5 μg m^{-3}, 300 μg m^{-3}, and 450 M m^{-1} within 4 h because the discharge of fireworks for celebrations. Wind speeds were only about 0.7 m s^{-1} during the period. Fig. 2 shows again that BC, Bsp, and $PM_{2.5}$ very similarly in time. The correlation coefficient (R) between BC and $PM_{2.5}$, between BC and Bsp, and between Bsp and $PM_{2.5}$ is 0.66, 0.85 and 0.74, respectively, suggesting the same emission sources for BC and $PM_{2.5}$ in Nanjing during the period.

To further understand the aerosol compositions in urban Nanjing, discontinuous samplings at the site were conducted during Phase 1 using Ambient Eight Stage Cascade Impactor Sampler. Table 2 lists the daily mean ratios of inorganic aerosols including sulfate, nitrate, and ammonium to total $PM_{2.1}$. Inorganic scattering aerosols in urban area of Nanjing account for about 49 ± 8.6% of total aerosols during this period (Table 2). At this site, nitrate concentration is larger than that of sulfate and this finding is in opposite to what is observed in a suburban site of Nanjing at the campus of Nanjing University of Information Science and Technology. The nitrate to sulfate ratio is about 1.24 in this urban site while it is only 0.9 in the suburban site. Larger nitrate to sulfate ratio in urban Nanjing may be caused by higher nitrate precursor emissions from vehicles (Zhu et al., 2012). Assuming that the ratio of each component in $PM_{2.1}$ were equal to that in $PM_{2.5}$ and the ratio is subsequently scaled seasonally from January to April, 2013, mean concentrations of sulfate, nitrate and ammonium in $PM_{2.5}$ in urban Nanjing could be estimated roughly to be 13.3, 16.4, and 7.2 μg m^{-3}, respectively.

In 2006 and 2007, atmospheric aerosols were measured at 14 sites, spreading over most regions of the mainland China (Zhang et al., 2008; X.Y. Zhang et al., 2012). Particularly, one of the sites was in LinAn (LA), a polluted rural site in YRD. The aerosol seasonality at the 14 sites was compared with this study, although it is understandable that the measurements for the 14 sites were made in earlier years. Fig. 3 shows the seasonal (from January to April) mean concentrations of BC and $PM_{2.5}$ as well as the ratio of BC to $PM_{2.5}$ over the 15 sites (including Nanjing in this study). The horizontal ordinate in Fig. 3 labels the abbreviations of the site names as listed in Table 3. High aerosol concentrations appear in southwestern, northern, and northeastern China, especially in urban sites. Both BC and $PM_{2.5}$ vary similarly in space over China. A site with high BC usually is also with high $PM_{2.5}$ and vice versa. Aerosol concentrations in urban Nanjing (NJ) are slightly higher than those in Nanning (NN) and Lhasa (LS) but much smaller than those at the other urban sites, such as Chengdu (CD), Panyu (PY), XiAn (XA), and Zhengzhou (ZZ). Compared with LA in YRD, Nanjing has a relatively higher $PM_{2.5}$ but a lower BC concentrations (Fig. 3). At most sites, ratios of BC to $PM_{2.5}$ ranged from 5 to 10% while the ratio in urban Nanjing was about 6%. As discussed in Zhang et al. (2009), emissions of aerosols and trace gases have kept increasing in the last decade. Comparison between recent and earlier observations of BC concentrations over China suggests that BC in LS and LA have increased considerably (Table 4). Aerosols concentrations in the 14 sites can be expected to increase in the recent years with increasing

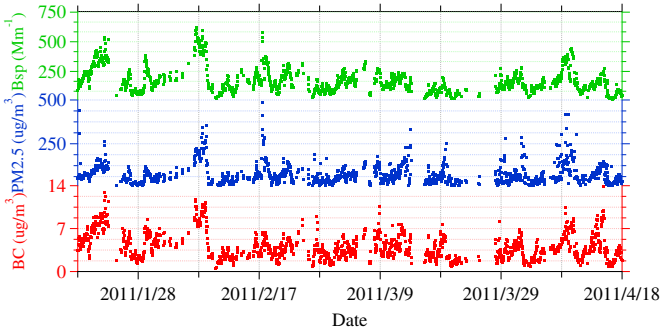

Fig. 1. Time series of aerosols from 18 January to 18 April in 2011 (Phase 1) in urban Nanjing. $PM_{2.5}$ scattering coefficient (Bsp, M m^{-1}), $PM_{2.5}$, and black carbon (BC) concentrations (μg m^{-3}) are indicated with green (top), blue (middle), and red (down) dots, respectively. (For interpretation of the references to colour in this figure legend, the reader is referred to the web version of this article.).

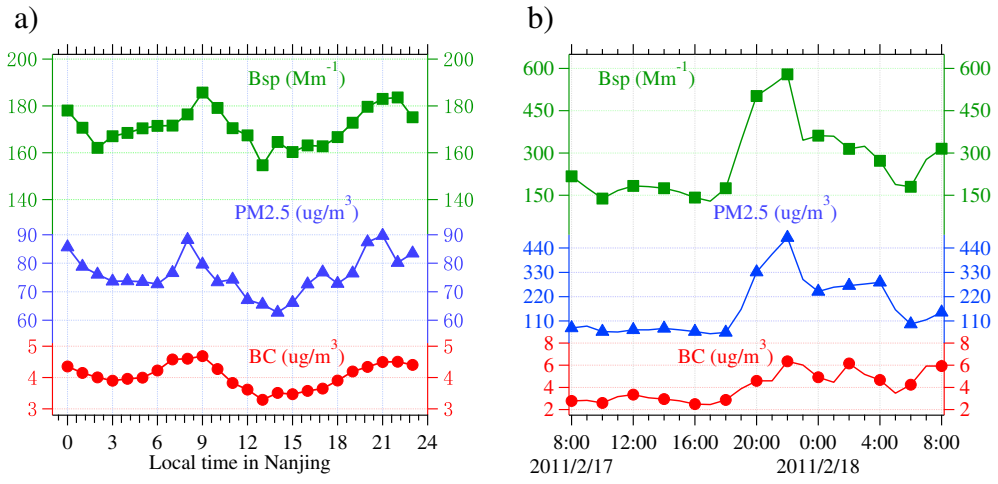

Fig. 2. Diurnal variations of Bsp (top, M m^{-1}), $PM_{2.5}$ (middle,μg m^{-3}) and BC concentrations (down, μg m^{-3}) averaged over Phase 1 from 18 January to 18 April in 2011 (a) and on a day during the Lantern Festivals with a pollution episode (b).

energy consumptions and economic activities. Therefore, the mean aerosol concentrations in urban Nanjing is still relatively low among the 15 sites over China or within YRD.

3.2. Optical properties of aerosols

Optical properties of aerosols in urban Nanjing is derived from one-year continuous measurements of aerosol optical properties, including optical depth of total (TAOD), absorbing (AAOD), fine (FAOD) and coarse (CAOD) aerosols, Angstrom exponent of total (TAE), absorbing (AAE) and fine (FAE) aerosols, and SSA of total aerosols during Phase 2.

Fig. 4 shows the seasonal mean wavelength-dependent TAOD, AAOD, FAOD and CAOD in urban Nanjing in spring (representing March, April and May hereinafter), summer (representing June, July, and August hereinafter), fall (representing September, October, and November hereinafter) and winter (representing December, January, and February hereinafter). TAOD, AAOD, and FAOD decreased with increasing wavelength while CAOD showed an opposite variation. For total, absorbing, and fine aerosols, the largest AOD appeared in summer possibly owing to high relative humidity (RH). CAOD in spring is higher than the other seasons possibly due to frequent dust storms at the times. For the same reason, TAOD in spring was also considerably large. Seasonal mean 550-nm AODs of total, absorbing, fine and coarse aerosols in urban Nanjing are listed in Table 5. The 550-nm AOD ranged 0.5–1.0 for TAOD, 0.04–0.05 for AAOD, 0.42–0.92 for FAOD, and 0.06–0.21 for CAOD. SSA, a quantity for radiative absorption capability of aerosols, is shown in Fig. 5 by wavelength and season. The mean SSA in urban Nanjing ranged from 0.90 to 0.95 in four seasons. Aerosols were more absorbing in fall possibly owing to the biomass burning in YRD (Zhuang et al., 2011). Lots of straw are burned in farmlands of YRD during the harvest seasons (such as in fall), which might emit considerable BC to the atmosphere (Zhuang et al., 2011). An increase in biomass burning would elevate BC concentrations and consequently enhance absorption of aerosols (Ramanathan and Carmichael, 2008). Annual mean SSA was about 0.92, 0.92, 0.91, and 0.90 at 440 nm, 675 nm, 870 nm, and 1020 nm, respectively.

The ground-based observations of AOD and SSA have much higher temporal resolutions than the satellite observation, while the latter has an advantage of global spatial coverage. Therefore, it is desirable to valid the satellite observation with the ground measurement. In Fig. 6, the surface observations of TAOD is compared with MODIS satellite data at 550-nm (Fig. 6a) and the surface observations of SSA is compared with Ozone Monitoring Instrument (OMI) satellite data at 440-nm (Fig. 6b). MODIS TAODs were found to be somewhat consistent with the ground-based observations. The majority of dots were concentrated around

Table 2
The ratios of sulfate, nitrate and ammonium to $PM_{2.1}$ in January, February, March, and April, 2011.

Month	Date	Sulfate	Nitrate	Ammonium	Total
Jan	04	0.12	0.16	0.09	0.37
	10	0.11	0.14	0.07	0.32
	18	0.14	0.19	0.09	0.41
Feb	16	0.25	0.15	0.08	0.49
	18	0.22	0.22	0.11	0.55
	21	0.17	0.28	0.11	0.57
Mar	01	0.17	0.28	0.10	0.55
	15	0.16	0.23	0.10	0.49
	18	0.21	0.21	0.10	0.52
Apr	02	0.15	0.28	0.10	0.53
	06	0.23	0.26	0.11	0.60
	11	0.17	0.18	0.07	0.43

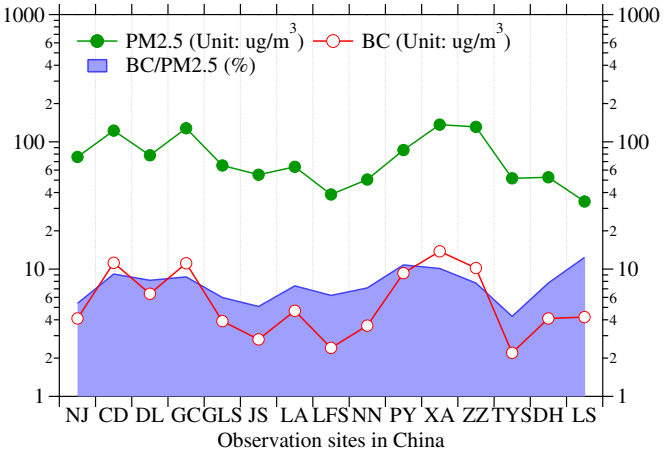

Fig. 3. BC and $PM_{2.5}$ concentrations and their ratios in urban Nanjing from this study in comparison with those at other 14 sites in China from Zhang et al., 2008; X.Y. Zhang et al., 2012. See Table 3 for the information on the sites, including the abbreviations for the site names in the horizontal coordinate.

Table 3
Sites information over China according to Zhang et al., 2008; X.Y. Zhang et al., 2012.

Sites	Full name	Lat (°N)	Lon (°E)	Descriptions
CD	Chengdu	30.65	104.04	Urban station, 496 m asl + 91 m-tall building
DL	Dalian	38.90	121.63	Urban station, 91 m asl + 5 m-tall building
DH	Dunhuang	40.15	94.68	Rural station, 1139 m asl + 5 m-tall building
GLS	Gaolanshan	36.00	105.85	Rural station, 1531 m asl + 544 m-tall hill
GC	Gucheng	39.13	115.80	Rural station, 15.2 m asl + 8 m-tall building
JS	Jinsha	29.63	114.20	Rural station, 416 m asl + 8 m-tall building
LS	Lhasa	29.67	91.13	Urban station, 3663 m asl
LA	LinAn	31.30	119.73	Rural station, 139 m asl + 10 m-tall building
LFS	Longfengshan	44.73	127.60	Rural station, 331 m asl + 6 m-tall building
NN	Nanning	22.82	108.35	Urban station, 84 m asl + 97 m-tall building
PY	Panyu	23.00	113.35	Urban station, 5 m asl + 140 m-tall hill
TYS	Taiyangshan	29.17	111.71	Rural station, 563 m asl + 8 m-tall building
XA	XiAn	34.43	108.97	Urban station, 363 m asl + 4 m-tall building
ZZ	Zhengzhou	34.78	113.68	Urban station, 99 m asl + 56, 5 and 10 m-tall buildings
NJ	Nanjing	32.05	118.78	Urban station, 20 m asl + 79.3 m-tall building

1:1 line. The correlation coefficient between MODIS and CIMEL AODs was 0.76. However, OMI-based SSA had a relatively weak correlation with CIMEL SSA (Fig. 6b), similar to the results from Liu and Hong (2012). Annual mean 550-nm TAOD from MODIS was about 0.74 ± 0.43. Annual mean 442-nm SSA of total aerosols from OMI was about 0.94 ± 0.2. Both AOD and SSA from satellites were slightly larger than the ground-based ones.

Fig. 7 shows seasonal variations of 675/440-nm total Angstrom Exponent (TAE), final aerosol Angstrom Exponent (FAE), and absorbing aerosol Angstrom Exponent (AAE). AOD and SSA are good indicators of aerosol loadings and absorbing ability and AE can describe the size of aerosols. Both AAE and FAE were the smaller in summer than in the other seasons. However, TAE was the smallest in spring possibly due to the effects of dust aerosol (see Fig. 4, CAOD was large in spring). The smallest median AE among four seasons was about 1.0 for total aerosols in spring, 1.4 for fine aerosols and 1.0 for absorbing aerosols in summer. Small FAE and AAE might be caused by large relative humidity (RH) (Fig. 8a). The median value of RH exceeded 70% in summer but was only about 45% in winter. Both AAE and FAE were anti-correlated with RH (Figs. 7b, c, and 8a). The correlation coefficient was −0.93 between AAE and RH and was −0.91 between FAE and RH (Fig. 8b). Therefore, large AODs in summer (Fig. 4) were likely resulted from the hygroscopic growth of the aerosols.

Table 4
Comparisons among observed BC (in μg m^{-3}) over China in earlier studies.

Sites (References)	Lat (°N)/Lon (°E)	Sampling time	Loadings
Nanjing (This study)	32.05/118.78	18th Jan to 18th Apr, 2011	4.1 ± 2.2
Waliguan (Tang et al., 1999)	36.30/100.90	Jan, 1995	0.22
Lhasa	29.67/91.13	Jun–Oct, 1998	0.3–4.8
(Qin et al., 2001)		Jun–Oct, 2006, 2007	1.6–5.2
(Zhang et al., 2008)			
Wenjiang (Qin et al., 2007)	30.97/103.8	Sep, 1999–Aug, 2000	1.24–19.12
Shangdianzi (Qin et al., 2001)	40.39/117.17	Sep, 1999–Mar, 2000	0.2–2.3
LinAn	31.30/119.73	Aug, 2000–Feb, 2001	1.44–7.5
(Qin et al., 2001)		Jan–Oct, 1991	2.3
(Tang et al., 1999)		Jan–Oct, 2006, 2007	4.3
(Zhang et al., 2008)			
Hok Tsui	22.20/114.25	Winter and	0.8 ± 0.3
(Duan et al., 2007)		Summer, 2002	and 1.4 ± 0.9
Lianyungang (Zhang et al., 2005)	34.59/119.16	Summer, 2003	3.8
Tongliao (Zhang et al., 2005)	41.59/122.49	Summer, 2003	2.0
Diqing (Qu et al., 2006)	27.80/100.00	Aug, 2004–Mar, 2005	0.34 ± 2.8

Table 6 summarized the annual mean AOD, SSA and AE of aerosols (Line 2–9 in the table) in urban Nanjing. AAOD was about one order of magnitude smaller than TAOD and FAOD. CAOD, which had a considerable standard deviation, was about 1/5 times to FAOD. Annual mean AAOD, FAOD, and CAOD was about 0.04 ± 0.02, 0.48 ± 0.29 and 0.11 ± 0.12, respectively. Annual mean aerosol SSA at 440 nm was about 0.92 ± 0.03. FAE was much larger than TAE. Annual mean AAE, FAE and TAE was 1.44 ± 0.5, 1.64 ± 0.29 and 1.25 ± 0.29, respectively.

Quality assessed aerosol data from AERONET at four sites in YRD were compared with our results. The four sites include Hefei (117.16°E, 31.91°N), Taihu (120.22°E, 31.42°N), Hangzhou (119.73°E, 30.26°N) and suburban Nanjing (118.72°E, 32.21°N). Table 6 lists 550-nm AOD and 675/440-nm AE in these sites (Line 10–17). In Taihu, the total aerosol AOD and AE were about 0.71 and 1.24 and have a similar seasonality to this study (not shown). The seasonal mean TAOD and TAE in Hangzhou were about 0.82 and 1.24 in fall 2007. Because of the presence of dust aerosols, the TAOD and TAE in suburban Nanjing were 0.63 and 0.81 in springs 2010. Our observation showed the similar results for urban Nanjing. Multi-year TAOD and TAE in Hefei were about 0.62 and 1.15 from 2005 to 2008. TAOD in YRD often exceed 0.6 and they are usually modulated by dust storms in spring.

3.3. Direct radiative forcing (DRF) of aerosols

When estimating the aerosol direct effect, surface albedo must be considered as its variation can alter the estimation greatly. The MODIS-based surface albedo by wavelength in urban Nanjing during Phase 2 is presented in Fig. 9, showing huge seasonal variations. The albedo in summer was larger than in other seasons. The surface albedo increased with wavelength in all seasons in the short-wave range. And it was lower than 0.15 in visible wavebands but higher than 0.2 in the longer wavebands in whole year (Fig. 9).

Fig. 10 shows the seasonal mean daytime clear sky DRFs of total and absorbing aerosols at the TOA and at the surface in urban Nanjing. Absorbing aerosol had a positive DRF at the TOA but a negative DRF at the surface. DRFs of total aerosols were negative both at the TOA and at the surface. Both total and absorbing aerosol DRFs show seasonal variations with stronger DRFs in summer than in the other seasons. Daytime DRF of absorbing aerosols was about 13.7 W m^{-2} at the TOA and −17.9 W m^{-2} at the surface in summer, while in winter, it was 7.2 at the TOA and −14.7 W m^{-2} at the surface. For total aerosols, daytime DRF was −15.5 W m^{-2} at the TOA and −55.1 W m^{-2} at the surface in summer, whereas the value in winter is −15.4 and −39.4 W m^{-2}, respectively, at the TOA and at the surface. It is noticeable that large ratio of the surface DRF to the TOA one was found in winter for absorbing aerosols while in summer for total aerosols. This was possibly because negative DRF of scattering aerosols in summer was substantially offset by very positive DRF of absorbing aerosols at the TOA. Mean diurnal variations of DRFs are shown in Fig. 11. There were two peaks (appeared

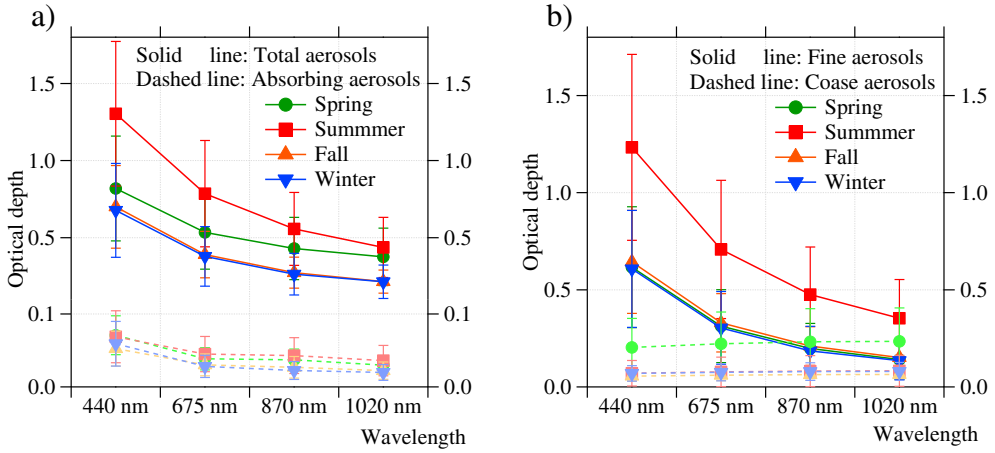

Fig. 4. Seasonal variations of wavelength-dependent AOD of total, absorbing (a), fine and coarse (b) aerosols in urban Nanjing from 22 April 2011 to 21 April 2012 (Phase 2).

at 9 am and 3 pm LST) for absorbing aerosol DRFs both at the TOA and surface within a day. The largest DRFs exceeded 12 W m^{-2} at the TOA while −20 W m^{-2} at the surface. Diurnal variations of total aerosol DRFs were different from those of absorbing aerosols'. At the TOA, the most negative DRF of total aerosols appeared at noon, with a minimum value of −22.7 W m^{-2}. At the surface, the DRF kept constant almost the whole daytime (9–16 LST) (Fig. 11b). Diurnal variation of total aerosol DRF somewhat followed that of absorbing aerosol DRF as negative forcing of the scattering aerosols was considerably offset by absorbing aerosols (Fig. 11a and b). Annual mean (including daytime and nighttime) DRFs of total and absorbing aerosols at the TOA were −6.9 and +4.5 W m^{-2}, respectively, and they were about −21.3 and −7.9 W m^{-2} at the surface.

Aerosol DRF over China has been a subject of numerous studies. Xia et al. (2007) reported that the daytime observed clear sky aerosol DRF at the surface in Taihu was about −38.4 W m^{-2}. Kuhlmann and Quaas (2010) found a reduction of shortwave radiation by 20–30 W m^{-2} due to aerosol perturbation over Qinghai-Tibet Plateau. This study suggested a more negative daytime surface DRF (−42.5 W m^{-2}) in urban Nanjing than these earlier studies. Table 7 briefly summarized the global, regional, and local aerosol TOA DRFs from observations and simulations. Aerosol DRFs under the clear sky is stronger than under all sky conditions. The global mean DRF of total aerosols in clear sky is estimated to be −5.4 W m^{-2} at the TOA from observation (Forster et al., 2007). This is much more negative than the simulation of −2.1 W m^{-2} by Reddy et al. (2005). At regional scale, the observed DRF of total aerosols in clear sky was positive in East Asia (Li et al., 2010), which it is negative, being −0.62 W m^{-2} (Zhuang et al., 2013b) and −0.2 W m^{-2} Han (2010) from simulations. Urban aerosols had much stronger DRFs than regional and global means as suggested in this and earlier studies (Alam et al., 2011) (Table 7).

Forster et al. (2007) suggested that the uncertainty of DRF derived from observations is much smaller than that from simulations because the current climate models perform poorly in describing aerosol mixings, profiles, and emissions (Ramanathan and Carmichael, 2008) and DRF is usually underestimated by these models. Ramanathan and Carmichael (2008) pointed out that aerosol absorption from observation is a factor of two or more larger than from the general circulation models (GCMs). The global mean BC DRF at the TOA is +0.9 W m^{-2} derived from observations, whereas it is only from +0.2 to +0.4 W m^{-2} from simulations Ramanathan and Carmichael (2008). A merging of modeled and observed aerosol parameters would reduce biases in simulations (Ramanathan and Carmichael, 2008). Clear sky TOA DRF of anthropogenic aerosols is −1.08 W m^{-2} by integrating satellite and ground-based observations with models (Chung et al., 2005). Absorbing aerosol DRF at the TOA in urban Nanjing is about 5 times of the global means.

3.3.1. *Sensitivities of DRF to surface albedo*

Surface albedo can affect aerosol DRF significantly (Ma and Yu, 2012). Brighter surfaces would reflect more solar radiation to the atmosphere and thus lead to more re-absorption and re-scattering of solar radiation by aerosols. To better understand the effects of

Table 5
Observed seasonal 550-nm AOD of total, absorbing, fine and coarse aerosols in urban Nanjing.

Factors	Spring	Summer	Fall	Winter
TAOD	0.65 ± 0.28	1.0 ± 0.4	0.52 ± 0.20	0.50 ± 0.24
AAOD	0.05 ± 0.02	0.05 ± 0.03	0.04 ± 0.02	0.04 ± 0.02
FAOD	0.43 ± 0.24	0.92 ± 0.41	0.45 ± 0.20	0.42 ± 0.23
CAOD	0.21 ± 0.16	0.07 ± 0.07	0.06 ± 0.03	0.07 ± 0.04

TAODAOD of total aerosols.
AAODAOD of absorbing aerosols.
FAODAOD of fine aerosols.
CAODAOD of coarse aerosols.

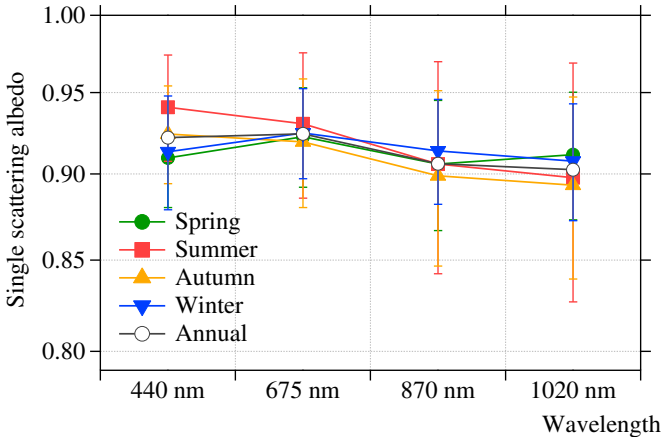

Fig. 5. Seasonal variations of total aerosol single scattering albedo (SSA) at 440, 675, 870 and 1020 nm in urban Nanjing from 22 April 2011 to 21 April 2012.

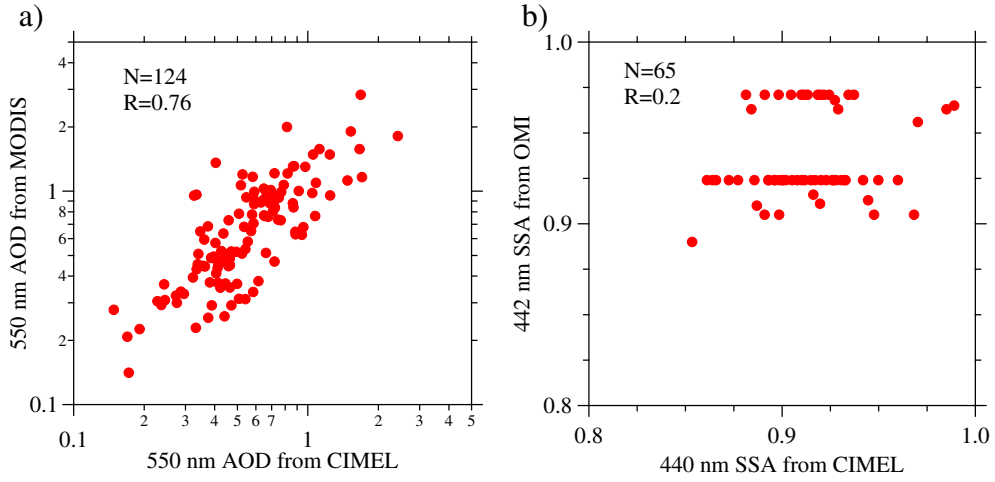

Fig. 6. Comparison between the surface-based and satellite-based (MODIS) 550-nm AOD (a, CIMEL-AOD vs. MODIS-AOD), and between the surface-based and satellite-based (OMI) 440-nm SSA (b, CIMEL-SSA vs OMI-SSA) in urban Nanjing.

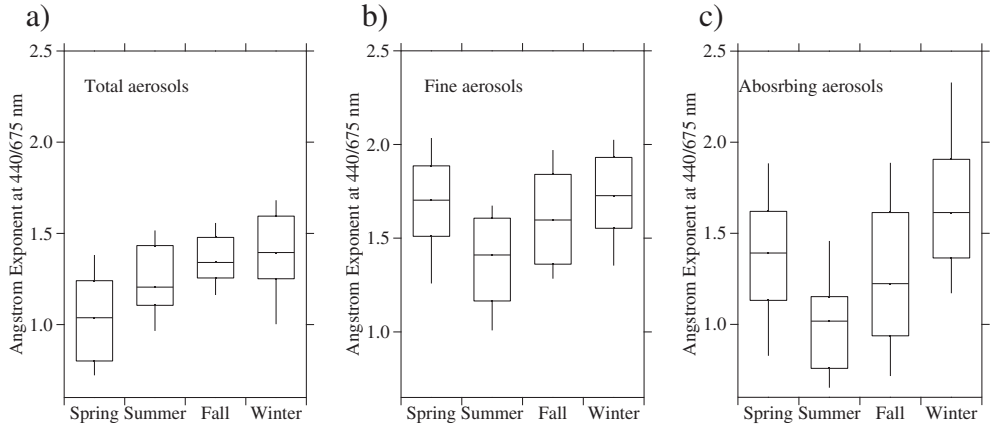

Fig. 7. Seasonal variations of Angstrom exponent (AE) of total (a), fine (b) and absorbing (c) aerosols in urban Nanjing from 22 Apr 2011 to 21 Apr 2012.

surface albedo on aerosol DRFs in urban Nanjing, sensitivity tests were carried out, in which surface albedo was set up as 0.04, 0.2, 0.25, and wavelength dependent (Fig. 11). Fig. 11 shows that TOA DRF becomes more positive with increases in surface albedo for absorbing aerosols but less negative for total aerosols, as with brighter surfaces, more solar radiation is absorbed by absorbing aerosols while less radiation is scattered by scattering aerosols in Earth-atmosphere system. These results are consistent with the

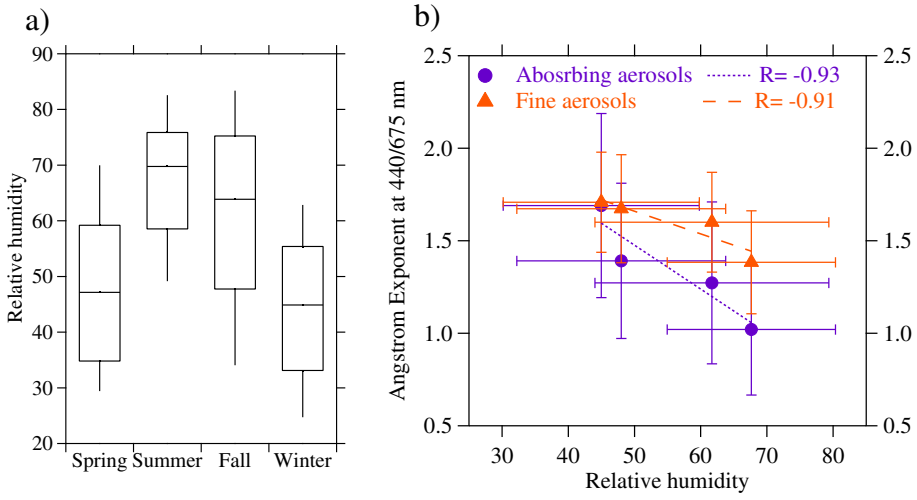

Fig. 8. Seasonal variations of relative humidity (RH, in %) (a) and linear correlations between seasonal mean RH and AE (b).

Table 6
Mean 550-nm AOD, 440-nm SSA, and 675/440-nm AE from observation in urban Nanjing.

Factors	Average	Std. dev.	Observation periods	Locations
TAOD	0.60	0.30	22 Apr 2011–21 Apr 2012	Urban Nanjing
AAOD	0.04	0.02		
FAOD	0.48	0.29		
CAOD	0.11	0.12		
SSA	0.92	0.03		
TAE	1.25	0.29		
FAE	1.64	0.29		
AAE	1.44	0.50		
TAOD	0.63	/	Mar, Apr 2010	Suburban Nanjing
TAE	0.81	/		
TAOD	0.71	/	22 Apr 2011–21 Apr 2012	Taihu
TAE	1.24	/		
TAOD	0.82	/	Fall 2007	Hangzhou
TAE	1.27	/		
TAOD	0.62	/	Nov 2005–Jan 2006;	Hefei
TAE	1.15	/	Dec 2007–May 2008; Aug 2008–Nov 2008	

TAODAOD of total aerosols.
AAODAOD of absorbing aerosols.
FAODAOD of fine aerosols.
CAODAOD of coarse aerosols.
TAEAE of total aerosols.
AAEAE of absorbing aerosols.
FAEAE of fine aerosols.

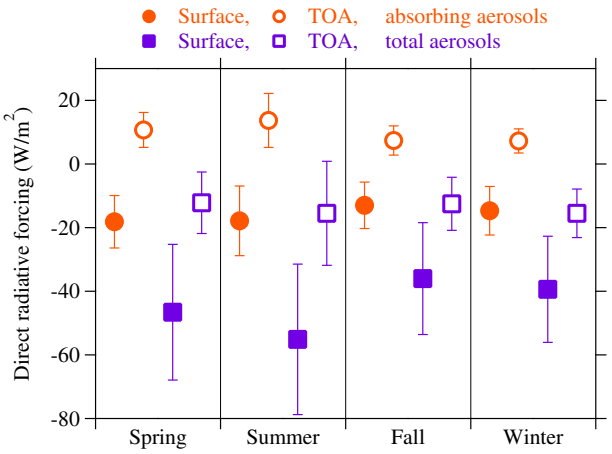

Fig. 10. Seasonal variations of daytime clear sky direct radiative forcing (DRF, W m^{-2}) of total and absorbing aerosols both at the TOA and surface in urban Nanjing from 22 Apr 2011 to 21 Apr 2012.

study of Stier et al. (2007). Changes in absorbing aerosol DRF at the surface were different from that at the TOA (Fig. 11a). Surface DRF of absorbing aerosols would become less negative with increasing surface albedo. When surface albedo was set to be 0.04, 0.2 and 0.25, corresponding daytime DRFs of total and absorbing aerosols were −30.6 and +3.0 W m^{-2}, −17.9 and +7.7 W m^{-2}, and −13.9 and +9.2 W m^{-2}, respectively, at the TOA in urban Nanjing. The strong warming effect of absorbing aerosols in urban Nanjing in summer (Fig. 10) was partially attributable to a brighter surface condition (Fig. 9) and thus offset more negative TOA DRF of scattering aerosols.

4. Conclusions

With the ground measurements and a radiation transfer model, we studied the characteristics, optical properties, and direct radiative forcing of aerosols in urban Nanjing, a megacity in Yangtze River Delta (YRD) of China.

We found that aerosols concentrations in the urban Nanjing are much lower than those at the other urban sites in China, such as Chengdu, Panyu, Xi'An, and Zhengzhou. From January to April, 2011 (Phase 1), $PM_{2.5}$ concentrations were about 76.1 ± 59.3 μg m^{-3}, with corresponding scattering coefficient of 170.9 ± 105.8 M m^{-1}. Inorganic scattering aerosols accounted for about 49 ± 8.6% of total aerosols while BC accounted for 6.6 ± 2.9%. BC concentrations were a little lower than that in a rural site of YRD. We found high pollution episodes in Spring and Lantern Festivals due to considerable discharge of fireworks. Composition analysis for Phase 1 indicates that nitrate is larger than sulfate in urban Nanjing.

One year measurements from 22 April 2011 to 21 April 2012 (Phase 2) show that annual mean 550-nm TAOD was 0.6 ± 0.3, which was about 0.07, 0.8 and 0.18 times of AAOD, FAOD and CAOD, respectively. Annual SSA of aerosols ranges from 0.90 to 0.92. As an indicator of aerosol sizes, 675/440-nm Angstrom exponent of total aerosols was about 1.25 ± 0.29, smaller than AAE (1.44) and FAE (1.64). TAOD, AAOD, FAOD, and aerosol sizes were larger in summer than in the other seasons, likely resulting from higher relative humidity then. Much smaller TAE and larger CAOD were mostly found in spring than in the other seasons due to frequent dust storms. AOD in urban Nanjing was lower than that in other sites in YRD such as in Hangzhou and Taihu. Among several populated cities in China (e.g., Chengdu, Panyu, XiAn, and Zhengzhou), AOD in urban Nanjing might be quite low.

Real time wavelength-dependent surface albedo from MODIS was applied to estimate aerosol DRFs in Nanjing. Due to aerosol absorption and scattering of shortwave radiation, energy budget of Earth-atmosphere system is modulated considerably in urban Nanjing, especially in summer. Annual mean clear sky DRFs (including daytime and nighttime) of absorbing and total aerosols were +4.5 and −6.9 W m^{-2}, respectively, at the TOA, while the values were −7.9 and −21.3 W m^{-2}, respectively, at the surface. Negative DRFs of total aerosols were greatly offset by absorbing aerosols. Ramanathan and Carmichael (2008) pointed out that climate models performed more poorly in aerosol DRFs than observation retrievals. Global mean DRF of absorbing aerosols from observations in Ramanathan and Carmichael (2008) was only about 1/5 of this study, reflecting the non-homogenous distribution of BC or absorbing aerosols. Global mean DRF of total aerosols summarized in the fourth IPCC report (Forster et al., 2007) is also smaller

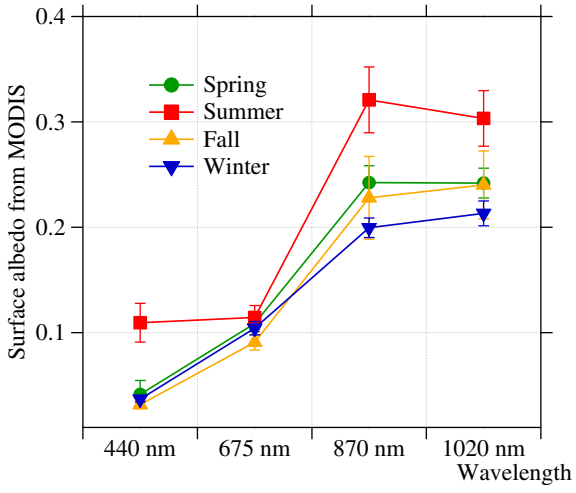

Fig. 9. Seasonal variations of wavelength-dependent surface albedo in Nanjing from 22 Apr 2011 to 21 Apr 2012.

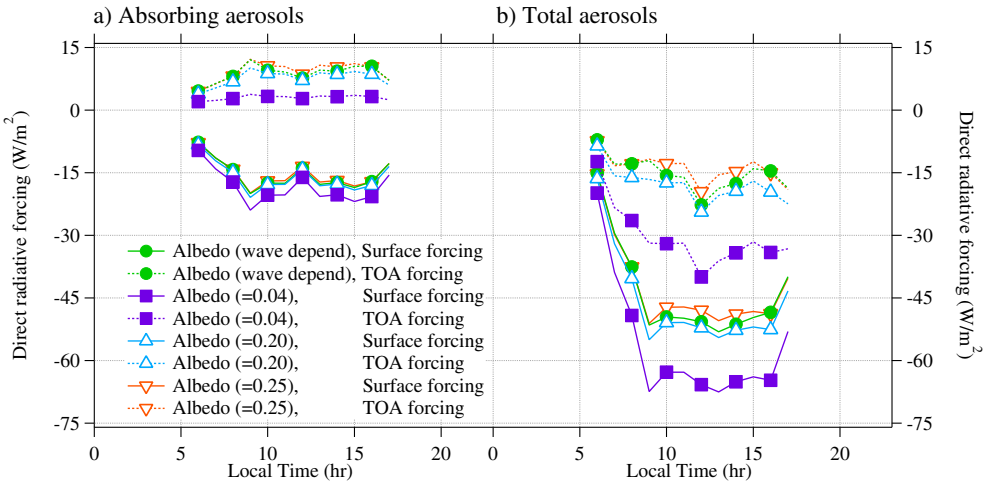

Fig. 11. Sensitivity of diurnal-aerosol DRFs (W m^{-2}) to surface albedo at the TOA and the surface in urban Nanjing for absorbing aerosols (a) and total aerosols (b).

Table 7
Comparison of direct radiative forcing (in W m^{-2}) at the TOA over China between this and earlier studies.

References	Methods	Scales	Species	DRF	
				All sky	Clear sky
This study	Observed	Urban Nanjing	Total aerosols	/	−6.9[a]
			Absorbing aerosols	/	+4.5[a]
Reddy et al. (2005)	Simulated	Global	Total aerosols	/	−2.1
Forster et al. (2007)	Observed	Global	Total aerosols	−0.55	−5.4[a]
Zhuang et al. (2013b)	Simulated	East Asia	Anthropogenic aerosols	−0.62	−4.97
Zhuang et al. (2013a)	Simulated	East Asia	Black carbon	+0.81	+1.2
Han (2010)	Simulated	East Asia	Total aerosols	−0.2	/
Li et al. (2010)	Observed	China	Total aerosols	/	0.3 ± 1.6[a]
Alam et al. (2011)	Observed	Urban Karachi	Total aerosol		−7–−35

[a] Including daytime and nighttime.

than that from this study. Both cooling effect of scattering aerosols and warming effect of absorbing aerosols are significant in urban Nanjing and within YRD, which should not be ignored. Our results also suggest that aerosol DRFs are sensitivity to surface albedo. In brighter surfaces, solar radiation is more absorbed by absorbing aerosols. Therefore, the warming effect of BC would become more significant if BC presents above the clouds, sea ice, and snow surface.

Acknowledgment

This work was supported by the National Key Basic Research Program of China (2011CB403406, 2014CB441203, 2010CB428503), the Young Scientist Fund of the National Natural Science Foundation of China (41205111), the New Teacher's Fund for Post Doctorial Program from the Chinese Ministry of Education (20120091120031), the Fundamental Research Funds for the Key Universities (1127020701), and the fund for the Priority Academic Program Development of Jiangsu Higher Education Institutions (PAPD). We thank the principal investigators and their teams for establishing and maintaining the sampling stations at Hangzhou, Hefei and Taihu. We also thank Nanjing University of Information Science and Technology (NUIST) for their assistance in analyzing the compositions of sampled particulate matters and for sharing their data with us. The constructive comments and suggestions from two anonymous reviewers are highly appreciated.

References

Alam, K., Trautmann, T., Blaschke, T., 2011. Aerosol optical properties and radiative forcing over mega-city Karachi. Atmos. Res. 101, 773–782.
Bai, H.T., Chen, Y.H., Wang, H.Q., Zhang, Q., Guo, N., Wang, S., Pan, H., Zhang, P., 2011. Seasonal variation of aerosol optical properties at AERONET of the semi-arid region in Loess Plateau. Arid Land Geogr. 34 (2), 1–8.
Bellouin, N., Boucher, O., Tanré, D., Dubovik, O., 2003. Aerosol absorption over the clear-sky oceans deduced from POLDER-1 and AERONET observations. Geophys. Res. Lett. 30 (14), 1748.
Cai, H.K., Zhou, R.J., Fu, Y.F., Zheng, Y.Y., Wang, Y.J., 2011. Cloud-aerosol lidar with orthogonal polarization detection of aerosol optical properties after a crop burning case. Clim. Environ. Res. 16 (4), 469–478.
Christopher, S.A., Zhang, J., Kaufman, Y.J., Remer, L., 2006. Satellite-based assessment of the top of the atmosphere anthropogenic aerosol radiative forcing over cloud-free oceans. Geophys. Res. Lett. 111, L15816.
Chung, C.E., Ramanathan, V., Kim, D., Podgorny, I.A., 2005. Global anthropogenic aerosol direct forcing derived from satellite and ground-based observations. J. Geophys. Res. 110, D24207.
Duan, J.C., Tan, J.H., Cheng, D.X., Bi, X.H., Deng, E.J., Sheng, G.Y., Fu, J.M., Wong, M.H., 2007. Sources and characteristics of carbonaceous aerosol in two largest cities in Pearl River Delta Region, China. Atmos. Environ. 41, 2895–2903.
Forster, P., Ramaswamy, V., Artaxo, P., Berntsen, T., Betts, R., Fahey, D.W., Haywood, J., Lean, J., Lowe, D.C., Myhre, G., Nganga, J., Prinn, R., Raga, G., Schulz, M., Van Dorland, R., 2007. Changes in atmospheric constituents and in radiative forcing. In: Solomon, S., et al. (Eds.), Climate Change 2007: the Physical Science Basis. Contribution of Working Group I to the Fourth Assessment Report of the Intergovernmental Panel on Climate Change. Cambridge Univ. Press, Cambridge, UK and New York, NY, USA, pp. 129–234.
Han, X., Zhang, M.G., Han, Z.W., Xin, J.Y., Liu, X.H., 2011. Simulation of aerosol direct radiative forcing with RAMS-CMAQ in East Asia. Atmos. Environ. 45 (36), 6576–6592.
Han, Z.W., 2010. Direct radiative effect of aerosols over East Asia with a regional coupled climate/chemistry model. Meteorol. Z. 19 (3), 287–298.
Han, Z.W., Li, J.W., Xia, X.A., Zhang, R.J., 2012. Investigation of direct radiative effects of aerosols in dust storm season over East Asia with an online coupled regional climate-chemistry-aerosol model. Atmos. Environ. 54, 688–699.
Han, X., Zhang, M.G., Liu, X.H., Ghan, S., Xin, J.Y., Wang, L.L., 2009. Development of RAMS-CMAQ to simulate aerosol optical depth and aerosol direct radiative forcing and its application to East Asia. Atmos. Ocean. Sci. Lett. 2 (6), 368–375.
Huang, Y., Chameides, W.L., Dickinson, R.E., 2007. Direct and indirect effects of anthropogenic aerosols on regional precipitation over East Asia. J. Geophys. Res. 112, D03212.
Jacobson, M.Z., 2001. Strong radiative heating due to the mixing state of black carbon in atmospheric aerosols. Nature 409, 695–697.
Jacobson, M.Z., 2002. Control of fossil-fuel particulate black carbon and organic matter, possibly the most effective method of slowing global warming. J. Geophys. Res. 107 (D19), 4410.
Khatri, P., Ishizaka, Y., Takamura, T., 2009. A study on aerosol optical properties in an urban atmosphere of Nagoya, Japan. J. Meteorol. Soc. Jpn. 87 (1), 19–38.
Kiehl, J.T., Briegleb, B.P., 1993. The relative roles of sulfate aerosols and greenhouse gases in climate forcing. Science 260, 311–314.
Kim, D., Wang, C., Ekman, A.M.L., Barth, M.C., Rasch, P.J., 2008. Distribution and direct radiative forcing of carbonaceous and sulfate aerosols in an interactive size-resolving aerosol–climate model. J. Geophys. Res. 113, D16309.
Kuhlmann, J., Quaas, J., 2010. How can aerosols affect the Asian summer monsoon? Assessment during three consecutive pre-monsoon seasons from CALIPSO satellite data. Atmos. Chem. Phys. 10, 4673–4688.

Li, Z.Q., Lee, K.H., Wang, Y.S., Xin, J.Y., Hao, W.M., 2010. First observation-based estimates of cloud-free aerosol radiative forcing across China. J. Geophys. Res. 115, D00K18.
Liao, H., Seinfeld, J.H., 2005. Global impacts of gas-phase chemistry-aerosol interactions on direct radiative forcing by anthropogenic aerosols and ozone. J. Geophys. Res. 110, D18208.
Liu, Q., Hong, Y.L., 2012. Comparison of aerosol single scattering albedo derived from the ozone monitoring instrument with aerosol robotic network observations. Atmos. Ocean. Sci. Lett. 5, 264–269.
Ma, X., Yu, F., 2012. Effect of spectral dependent surface albedo on Saharan dust direct radiative forcing. Geophys. Res. Lett. 39, L09808.
Madronich, S., 1993. UV radiation in the natural and perturbed atmosphere. In: Tevini, M. (Ed.), UV-B Radiation and Ozone Depletion. Effects on Humans, Animals, Plants, Microorganisms, and Materials. Lewis Publisher, Boca Raton, pp. 17–69.
Markowicz, K.M., Flatau, P.J., Remiszewska, J., Witek, M., Reid, E.A., Reid, J.S., Bucholtz, Z., Hilben, B., 2008. Observations and modeling of the surface aerosol radiative forcing during UAE. J. Atmos. Sci. 65, 2877–2891.
Palancar, G.G., Toselli, B.M., 2004. Effects of meteorology and tropospheric aerosols on UV-B radiation: a 4-year study. Atmos. Environ. 18, 2749–2757.
Penner, J.E., Andreae, M., Annegarn, H., Barrie, L., Feichter, J., Hegg, D., Jayaraman, A., Leaitch, R., Murphy, D., Nganga, J., Pitari, G., 2001. Aerosols, their direct and indirect effects. In: Houghton, J.T., et al. (Eds.), Climate Change 2001: the Scientific Basis. Contribution of Working Group I to the Third Assessment Report of the Intergovernmental Panel on Climate Change. Cambridge University Press, Cambridge, United Kingdom and New York, NY, USA, pp. 289–348.
Qin, S.G., Tang, J., Shi, G.Y., Wen, Y.P., 2007. Observational study of black carbon at Wenjiang, Sichuan Province. Acta Sci. Circumst. 27 (8), 1370–1376.
Qin, S.G., Tang, J., Wen, Y.P., 2001. Black carbon and its importance in climate change studies. Meteorol. Mon. 27 (11), 3–7.
Qu, W.J., Zhang, X.Y., Wang, Y.Q., Wang, D., Li, Y., Cao, G.L., Zhou, Y.M., 2006. The physical and chemical characterization of carbonaceous aerosol at the atmospheric background site in Diqing, Yunnan. China Environ. Sci. 26 (3), 266–270.
Ramanathan, V., Carmichael, G., 2008. Global and regional climate changes due to black carbon. Nat. Geosci. 1, 221–227.
Reddy, M.S., Boucher, O., Bellouin, N., Schulz, M., Balkanski, Y., Dufresne, J.L., Pham, M., 2005. Estimates of global multicomponent aerosol optical depth and direct radiative perturbation in the Laboratoire de Meteorologie Dynamique general circulation model. J. Geophys. Res. 110, D10S16.
Stier, P., Seifeld, J.H., Kinne, S., Boucher, O., 2007. Aerosol absorption and radiative forcing. Atmos. Chem. Phys. 7, 5237–5261.
Tang, J., Wen, Y.P., Zhou, L.X., 1999. Observational study of black carbon in clean air area of western China. Q. J. Appl. Meteorol. 10 (2), 160–170.
Wang, Y., Che, H.Z., Ma, J.Z., Wang, Q., Shi, G.Y., Chen, H.B., Goloub, P., Hao, X.J., 2009. Aerosol radiative forcing under clear, hazy, foggy, and dusty weather conditions over Beijing, China. Geophys. Res. Lett. 36, L06804.
Wang, T., Li, S., Shen, Y., Deng, J., Xie, M., 2010. Investigations on direct and indirect effect of nitrate on temperature and precipitation in China using a regional climate chemistry modeling system. J. Geophys. Res. 115, D00K26.
Wu, J., Fu, C.B., 2005. Simulation research of distribution transportation and radiative effects of black carbon aerosol in recent five spring seasons over East Asia region. Chin. J. Atmos. Sci. 29 (1), 111–119.
Xia, X.A., Li, Z.Q., Holben, B., Wang, P., Eck, T., Chen, H.B., Cribb, M., Zhao, Y.X., 2007. Aerosol optical properties and radiative effects in the Yangtze Delta region of China. J. Geophys. Res. 112, D22S12.
Xiao, Z.Y., Jiang, H., Chen, J., Wang, B., Jiang, Z.S., 2011. Monitoring the aerosol optical properties over Hangzhou using remote sensing data. Acta Sci. Circumst. 31 (8), 1758–1767.
Yan, P., Liu, G.Q., Zhou, X.J., Wang, J.L., Tang, J., Liu, Q., Wang, Z.F., Zhou, H.G., 2010. Characteristics of aerosols optical properties during haze and fog episodes at Shangdianzi in Northern China. J. Appl. Meteorol. Sci. 21 (3), 257–265.
Yu, H., Kaufman, Y.J., Chin, M., Feingold, G., Remer, L.A., Anderson, T.L., Balkanski, Y., Bellouin, N., Boucher, O., Christopher, S., DeCola, P., Koch, R., Loeb, N., Reddy, M.S., Schulz, M., Takemura, T., Zhou, M., 2006. A review of measurement-based assessments of the aerosol direct radiative effect and forcing. Atmos. Chem. Phys. 6, 613–666.
Zhang, H., Shen, Z., Wei, X., Zhang, M., Li, Z., 2012. Comparison of optical properties of nitrate and sulfate aerosol and the direct radiative forcing due to nitrate in China. Atmos. Res. 113, 113–125.
Zhang, Q., Streets, D.G., Carmichael, G.R., He, K.B., Huo, H., Kannari, A., Klimont, Z., Park, I.S., Reddy, S., Fu, J.S., Chen, D., Duan, L., Lei, Y., Wang, L.T., Yao, Z.L., 2009. Asian emissions in 2006 for the NASA INTEX-B mission. Atmos. Chem. Phys. 9, 5131–5153.
Zhang, X.Y., Wang, Y.Q., Niu, T., Zhang, X.C., Gong, S.L., Zhang, Y.M., Sun, T.Y., 2012. Atmospheric aerosol compositions in China: spatial/temporal variability, chemical signature, regional haze distribution and comparisons with global aerosols. Atmos. Chem. Phys. 12, 779–799.
Zhang, X.Y., Wang, Y.Q., Wang, D., Gong, S.L., Arimoto, R., Mao, L.J., Li, J., 2005. Characterization and sources of regional-scale transported carbonaceous and dust aerosols from different pathways in coastal and sandy land areas of China. J. Geophys. Res. 110, D15301.
Zhang, X.Y., Wang, Y.Q., Zhang, X.C., Guo, W., Gong, S.L., 2008. Carbonaceous aerosol composition over various regions of China during 2006. J. Geophys. Res. 113, D14111.
Zhou, B., Zhang, L., Cao, X.J., Han, X., Zhang, W., Feng, G.H., 2011. Analyses on atmospheric aerosol optical properties with lidar data in Lanzhou suburb. Plateau Meteorol. 30 (4), 1011–1017.
Zhu, J.L., Wang, T.J., Talbot, R.H., Mao, H.T., Hall, C.B., Yang, X.Q., Fu, C.B., Zhuang, B.L., Li, S., Han, Y., Huang, X., 2012. Characteristics of atmospheric Total Gaseous Mercury (TGM) observed in urban Nanjing, China. Atmos. Chem. Phys. 12, 12103–12118.
Zhuang, B.L., Jiang, F., Wang, T.J., Li, S., Zhu, B., 2011. Investigation on the direct radiative effect of fossil fuel black-carbon aerosol over China. Theor. Appl. Climatol. 104 (3–4), 301–312.
Zhuang, B.L., Liu, Q., Wang, T.J., Yin, C.Q., Li, S., Xie, M., Jiang, F., Mao, H.T., 2013a. Investigation on semi-direct and indirect climate effects of fossil fuel black carbon aerosol over China. Theor. Appl. Climatol.. http://dx.doi.org/10.1007/s00704-013-0862-8.
Zhuang, B.L., Li, S., Wang, T.J., Deng, J.J., Xie, M., Yin, C.Q., Zhu, J.L., 2013b. Direct radiative forcing and climate effects of anthropogenic aerosols with different mixing states over China. Atmos. Environ. 79, 349–361.